Journal of Alloys and Compounds 498 (2010) 42–51

Contents lists available at ScienceDirect

Journal of Alloys and Compounds

journal homepage: www.elsevier.com/locate/jallcom

Crystal chemistry, Rietveld refinements and Raman spectroscopy studies of the new solid solution series: $Ba_{3-x}Sr_x(VO_4)_2$ ($0 \le x \le 3$)

M. Azdouz[a,c], Bouchaib Manoun[a,*], R. Essehli[b], M. Azrour[a], L. Bih[a], S. Benmokhtar[d], A. Aït Hou[c], P. Lazor[e]

[a] Laboratoire de Physico-Chimie des Matériaux, Département de Chimie, FST Errachidia, Morocco
[b] SUBATECH, Unité Mixte de Recherche 6457, École des mines de Nantes, CNRS/IN2P3, Université de Nantes, BP 20722, 44307 Nantes Cedex 3, France
[c] Laboratoire des ressources naturelles et environnement, FST Errachidia, Morocco
[d] Laboratory of Chemistry of Solid Materials, Department of Chemistry, Faculty of Sciences Ben M'Sik Casablanca, Morocco
[e] Department of Earth Sciences, Uppsala University, S-752 36 Uppsala, Sweden

ARTICLE INFO

Article history:
Received 21 December 2009
Received in revised form 2 March 2010
Accepted 3 March 2010
Available online 11 March 2010

Keywords:
Orthovanadates
X-ray diffraction
Rietveld refinements
Raman spectroscopy
$Ba_{3-x}Sr_x(VO_4)_2$

ABSTRACT

The new solid solution series $Ba_{3-x}Sr_x(VO_4)_2$ ($0 \le x \le 3$) has been synthesized and studied by a combination of X-ray powder diffraction and Raman vibrational spectroscopy. This continuous solid solution crystallise in the hexagonal system with $R\bar{3}m$ space group. The structure has been determined at room temperature from X-ray diffraction by the Rietveld method analysis. It is formed by a 3D network of $(Ba/Sr)_{(1)}(VO_4)_2^{4-}$ layers linked into a crystal network by $(Ba/Sr)^{2+}_{(2)}$ cations. The vibrational spectra of this crystalline orthovanadate solid solution series are interpreted by means of factor group analysis in terms of space group $R\bar{3}m$ (D^5_{3d}). Assignments of the V–O vibrational stretching and bending modes, as well as some of the external modes, have been made. While all the modes show a monotonous shift as a function of the composition x, a break in the curves of intensities, full width at half maximum and band areas as a function of x is observed and attributed to the statistical distribution of Ba and Sr ions in the same crystallographic sites.

1. Introduction

The alkaline earth metal orthovanadates, $A_3(VO_4)_2$ (A = Ca, Sr, Ba), have attracted much attention owing to their interesting optical, transport, and ferroelectric properties [1–7]. Among them, strontium and barium orthovanadates, $Sr_3(VO_4)_2$ and $Ba_3(VO_4)_2$, exhibit intense rare earth activated luminescence and can be used in television tubes, luminescent lamp coatings and solid state lasers [1–3]. Because of the importance of these materials, recently Ni et al. reported on the synthesis, characterization and optical property of $Zn_3(VO_4)_2$ [8], the material exhibit excellent visible light emission ranging from 500 to 700 nm. Cao et al. reported on the photoluminescence properties of $Ca_9Y(VO_4)_7$ and $Ca_9Y_{0.95}Ln_{0.05}(VO_4)_7$ ($Ln^{3+} = Eu^{3+}$, Sm^{3+}, Pr^{3+}) [9], their results indicate that $Ca_9Y(VO_4)_7$ is a potential host material for Eu^{3+}, Sm^{3+} and Pr^{3+}. Umemura et al. studied the low-temperature sintering-microwave dielectric property relations in $Ba_3(VO_4)_2$ ceramic [10]. Sobczyk reported on synthesis and optical properties of $KZnLa_{0.99}Nd_{0.01}(VO_4)_2$ material, it strongly emits in the near infrared range, they claim that this type of compounds could be a new promising laser materials [11]. The structure of strontium and barium tetraoxovanadates (V), $Sr_3(VO_4)_2$ and $Ba_3(VO_4)_2$ with space group $R\bar{3}m$, can be derived from the structure of $K_2Pb(SO_4)_2$ palmierite [12,13]. It is comprised of $[Me_{(1)}(VO_4)_2]^{4-}$ layers linked into a crystal network by $Me^{2+}_{(2)}$ cations. Manoun et al. and Popovic et al. reported previously on the solid solution between isostructural phosphates substituting barium with strontium in $Ba_3(PO_4)_2$:$Ba_{3-x}Sr_x(PO_4)_2$ [14,15]. Using Raman spectroscopy and X-ray diffraction techniques, the results showed continuous solid solutions. Because of the fascinating structures and optical properties of these type of materials and specially orthovanadates we would like to continue with our investigations in similar compounds, the main object of this paper is the crystal chemistry, Rietveld refinements and Raman spectroscopy studies of $Ba_{3-x}Sr_x(VO_4)_2$ series ($0 \le x \le 3$).

2. Experimental

2.1. Synthesis

$Ba_{3-x}Sr_x(VO_4)_2$ orthovanadate powders were prepared by usual solid state techniques from powdered mixtures of $BaCO_3$, $SrCO_3$ and NH_4VO_3 in the adequate stoichiometric ratios according to the reaction:

$$(3-x)BaCO_3 + xSrCO_3 + 2NH_4VO_3 \rightarrow Ba_{3-x}Sr_x(VO_4)_2 + 3CO_2 + 2NH_3 + H_2O$$

* Corresponding author.
E-mail address: manounb@gmail.com (B. Manoun).

0925-8388/$ – see front matter © 2010 Elsevier B.V. All rights reserved.
doi:10.1016/j.jallcom.2010.03.066

Table 1
Unit cell parameters of $Ba_{3-x}Sr_x(VO_4)_2$, $0 \le x \le 3$.

	Rietveld parameters			DICVOL parameters			
	a (Å)	c (Å)	c/a	a (Å)	c (Å)	$M_{(20)}$	$F_{(20)}$
$Ba_3(VO_4)_2$	5.7811(1)	21.2886(4)	3.6824	5.7794	21.2872	50.7	40.8
$Ba_{2.5}Sr_{0.5}(VO_4)_2$	5.7617(1)	21.1048(3)	3.6629	5.7611	21.1095	28.8	20.5
$Ba_2Sr(VO_4)_2$	5.7362(1)	20.9041(4)	3.6442	5.7353	20.9055	32.7	27.7
$Ba_{1.5}Sr_{1.5}(VO_4)_2$	5.7084(1)	20.6912(4)	3.6247	5.7069	20.7031	15.0	15.4
$BaSr_2(VO_4)_2$	5.6792(1)	20.4821(4)	3.6065	5.6812	20.4806	31.0	28.0
$Ba_{0.5}Sr_{2.5}(VO_4)_2$	5.6498(1)	20.2789(3)	3.5893	5.6480	20.2446	10.0	10.1
$Sr_3(VO_4)_2$	5.6214(1)	20.0997(3)	3.5756	5.6188	20.0508	30.6	19.4

Each mixture was preheated in aluminium crucible at 300 °C for 2 h to decompose the ammonium vanadate, then ground in an agate mortar and heated, in 50 °C steps, in air between 400 and 600 °C for 72 h. The resulting powder was ground again and heated up to 850 °C for 18 h. On the final white products X-ray powder diffraction analysis was performed using CuKα radiation.

2.2. Instrumental methods

2.2.1. X-ray diffraction

The structural refinements were undertaken from the powder data. Diffraction data were collected at room temperature on a phillips D 5000 (θ–θ) diffractometer: Bragg–Brentano geometry; diffracted-beam graphite monochromator; CuKα radiation (40 kV, 40 mA); Soller slits of 0.02 rad on incident and diffracted-beams; divergence slit of 0.5°; antiscatter slit of 1°; receiving slit of 0.1 mm; with sample spinner. The patterns were scanned through steps of 0.01 (2θ), between 10° and 100° (2θ) with a fixed-time counting of 10–30 s. The full pattern refinements were carried out by means of the Rietveld method using the FULLPROF program [16] integrated in WINPLOTR software [17].

2.2.2. Raman spectroscopy

The Raman spectra were recorded with an imaging spectrometer (HoloSpec f/1.8i, Kaiser Optical Systems) equipped with a holographic transmission grating and thermoelectrically cooled two-dimensional multichannel CCD detector (Newton, Andor Technology, 1600 × 400 pixels, −60 °C) (see ref. [18] for more details). Non-polarized Raman spectra were collected in the back-scattering geometry, in the range 180–2280 cm^{-1}, at a resolution of about 3 cm^{-1}. Accuracy of spectral measurements, resulting from the wavelength calibration procedure and experimental conditions, is estimated to be about 1.5 cm^{-1}. Precision of the reported peak positions, as represented by standard errors obtained in peak fits, varied between

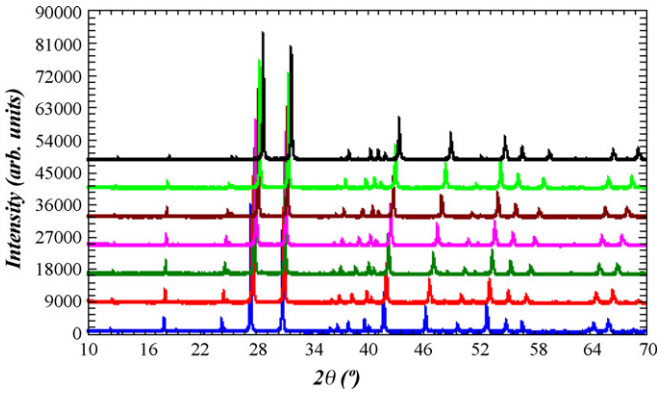

Fig. 1. X-ray powder diffraction patterns for $Ba_{3-x}Sr_x(VO_4)_2$ ($0 \le x \le 3$), bottom pattern ($x = 0$) and upper pattern ($x = 3$).

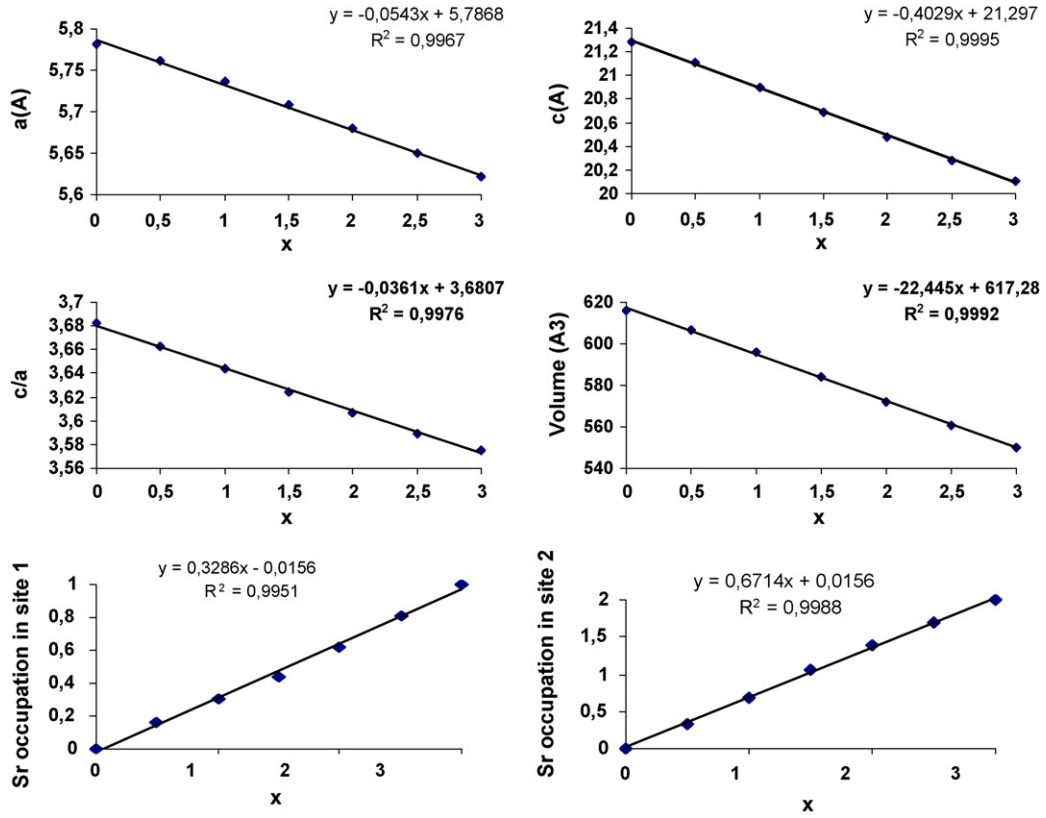

Fig. 2. Cell parameter variations as a function of x for $Ba_{3-x}Sr_x(VO_4)_2$ ($0 \le x \le 3$), where progressive substitution of barium by strontium provokes a decrease of the unit cell parameters a, c and V. Also we plot in this figure the Ba/Sr site occupation as a function of x.

Table 2
X-Ray powder diffraction data observed and calculated for $Ba_{3-x}Sr_x(VO_4)_2$, λ(CuKα$_1$) = 1.5406 Å.

h k l	$Ba_3(VO_4)_2$				$Ba_{2.5}Sr_{0.5}(VO_4)_2$				$Ba_2Sr(VO_4)_2$			
	d_{calc} (Å)	d_{obs} (Å)	I_{obs}	I_{calc}	d_{calc} (Å)	d_{obs} (Å)	I_{obs}	I_{calc}	d_{calc} (Å)	d_{obs} (Å)	I_{obs}	I_{calc}
0 0 3	7.0962	7.1120	1	1	7.0349	7.0247	1	1	6.9680	6.9663	1	2
1 0 1	4.8736	4.8777	9	10	4.8559	4.8442	8	9	4.8331	4.8309	8	8
1 0 4	3.6466	3.6507	12	11	3.6254	3.6186	11	10	3.6005	3.5982	9	8
0 1 5	3.2434	3.2450	100	100	3.2226	3.2176	100	100	3.1987	3.1973	100	100
1 1 0	2.8905	2.8920	88	85	2.8809	2.8765	88	86	2.8681	2.8666	89	89
0 2 1	2.4862	2.4872	3	3	2.4777	2.4746	3	3	2.4665	2.4652	2	3
2 0 2	2.4368	2.4380	6	6	2.4280	2.4245	7	6	2.4165	2.4148	6	6
0 0 9	2.3654	2.3663	8	8	2.3450	2.3424	8	8	2.3227	2.3221	7	7
0 1 8	2.3498	2.3513	1	2	2.3322	2.3311	2	2	2.3126	2.3107	2	2
0 2 4	2.2652	2.2664	11	11	2.2555	2.2532	11	11	2.2435	2.2418	10	10
1 1 6	2.2410	2.2423	5	6	2.2288	2.2263	5	6	2.2143	2.2138	5	6
2 0 5	2.1579	2.1588	41	43	2.1478	2.1451	42	42	2.1354	2.1317	42	43
1 0 1 0	1.9591	1.9602	27	26	1.9438	1.9421	26	26	1.9268	1.9246	26	25
0 2 7	1.9328	1.9343	2	2	1.9222	1.9206	1	2	1.9096	1.9091	2	2
2 1 1	1.8849	1.8860	2	3	1.8785	1.8773	2	2	1.8701	1.8687	2	2
1 1 9	1.8306	1.8315	10	11	1.8187	1.8172	9	10	1.8050	1.8030	8	8
2 1 4	1.7830	1.7834	3	3	1.7759	1.7745	3	2	1.7670	1.7653	2	2
1 2 5	1.7292	1.7299	31	31	1.7219	1.7206	30	30	1.7128	1.7108	28	30
3 0 0	1.6689	1.6693	15	16	1.6633	1.6621	15	16	1.6559	1.6542	15	16
0 2 1 0	1.6217	1.6225	12	11	1.6113	1.6103	11	11	1.5994	1.5974	11	11
0 3 6	1.5102	1.5109	1	1	1.5036	1.5021	1	1	1.4956	1.4952	1	1
2 2 0	1.4453	1.4456	13	14	1.4404	1.4390	14	14	1.4340	1.4321	14	14
2 1 1 0	1.4143	1.4149	17	18	1.4063	1.4049	17	17	1.3969	1.3946	17	17
0 3 9	1.3636	1.3641	2	2	1.3567	1.3436	2	2	1.3483	1.3477	2	1

h k l	$Ba_{1.5}Sr_{1.5}(VO_4)_2$				$BaSr_2(VO_4)_2$				$Ba_{0.5}Sr_{2.5}(VO_4)_2$			
	d_{calc} (Å)	d_{obs} (Å)	I_{obs}	I_{calc}	d_{calc} (Å)	d_{obs} (Å)	I_{obs}	I_{calc}	d_{calc} (Å)	d_{calc} (Å)	I_{obs}	I_{calc}
0 0 3	6.8971	6.9124	1	1	6.8274	6.8464	1	1	6.7596	6.8077	1	1
1 0 1	4.8083	4.8171	7	7	4.7824	4.7947	6	6	4.7564	4.7788	4	4
1 0 4	3.5740	3.5781	8	7	3.5471	3.5537	7	5	3.5206	3.5335	5	4
0 1 5	3.1732	3.1730	100	100	3.1476	3.1510	100	100	3.1225	3.1336	100	100
1 1 0	2.8542	2.8556	92	91	2.8396	2.8420	92	93	2.8249	2.8336	98	96
0 2 1	2.4544	2.4563	2	3	2.4416	2.4439	2	2	2.4288	2.4341	2	2
2 0 2	2.4041	2.4056	6	6	2.3912	2.3929	6	7	2.3782	2.3842	8	8
0 0 9	2.2990	2.3012	7	7	2.2758	2.2765	7	7	2.2532	2.2565	6	7
0 1 8	2.2917	2.2917	2	2	2.2710	2.2625	2	2	2.2507	2.2507	3	3
0 2 4	2.2303	2.2309	10	10	2.2168	2.2197	9	9	2.2033	2.2088	9	10
1 1 6	2.1988	2.1999	5	6	2.1830	2.1861	5	6	2.1675	2.1727	6	6
2 0 5	2.1221	2.1224	44	45	2.1084	2.1088	42	44	2.0948	2.0980	45	48
1 0 1 0	1.9087	1.9084	27	26	1.8908	1.8912	26	26	1.8734	1.8755	29	29
0 2 7	1.8962	1.8857	1	1	1.8826	1.8886	1	1	1.8691	1.8691	1	1
2 1 1	1.8609	1.8616	2	2	1.8513	1.8532	1	2	1.8417	1.8447	1	1
1 1 9	1.7904	1.7915	7	8	1.7758	1.7778	5	6	1.7615	1.7650	5	5
2 1 4	1.7574	1.7574	2	2	1.7474	1.7489	2	1	1.7374	1.7408	1	1
1 2 5	1.7030	1.7021	30	31	1.6928	1.6944	29	30	1.6827	1.6855	32	33
3 0 0	1.6479	1.6487	16	17	1.6394	1.6408	16	16	1.6310	1.6335	18	18
0 2 1 0	1.5866	1.5876	11	11	1.5738	1.5755	11	11	1.5613	1.5634	13	12
0 3 6	1.4868	1.4873	1	1	1.4778	1.4788	1	1	1.4689	1.4711	1	1
2 2 0	1.4271	1.4275	15	15	1.4198	1.4208	14	14	1.4125	1.4141	17	17
0 1 1 4	1.4160	1.4164	2	2	1.4023	1.4042	2	2	1.3889	1.3910	1	1
2 1 1 0	1.3868	1.3873	18	18	1.3765	1.3775	16	17	1.3665	1.3683	19	20

$Sr_3(VO_4)_2$

h k l	d_{calc} (Å)	d_{obs} (Å)	I_{obs}	I_{calc}	*h k l*	d_{calc} (Å)	d_{obs} (Å)	I_{obs}	I_{calc}
0 0 3	6.6999	6.6841	1	1	1 0 0	1.8579	1.8569	29	29
1 0 1	4.7315	4.7262	2	3	0 2 7	1.8568	1.8528	1	1
1 0 4	3.4965	3.4913	3	2	2 1 1	1.8324	1.8324	1	1
0 1 5	3.0998	3.0960	100	100	1 1 9	1.7485	1.7475	4	4
1 1 0	2.8107	2.8070	98	94	1 2 5	1.6731	1.6721	30	30
0 2 1	2.4165	2.4130	1	1	3 0 0	1.6228	1.6219	17	17
2 0 2	2.3658	2.3634	8	8	0 2 1 0	1.5499	1.5493	12	11
0 0 9	2.2333	2.2332	6	6	1 2 8	1.4846	1.4842	1	1
0 1 8	2.2327	2.2314	3	3	2 0 1 1	1.4613	1.4606	1	1
0 2 4	2.1907	2.1888	8	9	2 2 0	1.4054	1.4046	16	16
1 1 6	2.1532	2.1517	5	6	0 1 1 4	1.3771	1.3768	1	1
2 0 5	2.0822	2.0804	45	47	2 1 1 0	1.3572	1.3566	19	19

Table 3
Refinement conditions (X-ray powder data) for some compositions of $Ba_{3-x}Sr_x(VO_4)_2$ series.

	$x=0$	$x=0.5$	$x=1$	$x=1.5$	$x=2$	$x=2.5$	$x=3$
Wavelength (Å)	$\lambda_{k\alpha1}=1.5406$, $\lambda_{k\alpha2}=1.54439$						
Step scan increment (°2θ)	0.01						
Program	FULLPROF						
Space group	$R\bar{3}m$						
2θ range (°)	5–110	10–99	10–97	10–100	10–93	10–100	10–100
Zero point (°2θ)	−0.0268(9)	0.0292(8)	0.0108(10)	−0.0400 (8)	−0.0634(9)	−0.1164(8)	0.0305(7)
No. of reflections	263	218	207	214	186	202	195
No. of refined parameters	27	28	28	28	28	28	27
Pseudo-Voigt function	$\eta=0.72$ (2)	0.57 (1)	0.73 (2)	0.81 (2)	0.68 (2)	0.70(2)	0.87 (2)
$PV=\eta L+(1-\eta)G$							
Caglioti parameters							
U	0.030(3)	0.038(3)	0.074(4)	0.067(4)	0.052(4)	0.044 (4)	0.042 (3)
V	0.006(3)	0.014(3)	−0.009(4)	−0.001(3)	0.006(4)	0.010 (3)	0.005 (3)
W	0.004(1)	0.009(1)	0.007(1)	0.004(1)	0.004(1)	0.003 (1)	0.003 (1)
Reliability factors							
Rp	5.52	4.87	6.53	6.09	5.47	5.54	6.11
Rwp	7.43	6.63	9.00	8.36	7.81	7.70	8.50
cRp	11.3	10.1	13.5	12.8	10.8	11.3	11.5
cRwp	12.2	10.9	14.7	13.8	12.3	12.4	13.0
R_B	4.13	3.14	3.53	3.42	3.18	3.63	4.04
R_F	3.32	2.80	3.30	3.05	3.10	3.42	4.35

0.04 and 0.7 cm^{-1}, depending on the signal-to-noise ratio and peak overlap. The acquisition time varied from 4 to 5 s.

3. Results and discussion

3.1. X-ray powder diffraction patterns analysis

Fig. 1 shows the X-ray powder diffraction patterns of $Ba_{3-x}Sr_x(VO_4)_2$ series ($0 \le x \le 3$), the patterns are similar to those of the end members $Ba_3(VO_4)_2$ and $Sr_3(VO_4)_2$ and reveal the existence of a single phase type $Ba_3(VO_4)_2$ and $Sr_3(VO_4)_2$ which are isostructural. Indexing of X-ray powder diffraction patterns for these compositions was performed by means of the computer program DICVOL [19]. The first 20 peak positions, with a maximal absolute error of 0.03° (2θ), were used as input data. The X-ray diffraction pattern for all the compositions was assigned to a hexagonal structure adopting $R\bar{3}m$ as a space group. The lattice parameters were refined using the complete powder diffraction data sets and the complete powder diffraction data and intensities are given in Table 1. The values of the figures of merit (M_{20} and F_N [19]) (Table 2) are an indicator of the patterns quality. All the observed reflections for the compositions could be indexed in the space group $R\bar{3}m$ (no. 166).

Fig. 2 shows the cell parameter variations as a function of x for $Ba_{3-x}Sr_x(VO_4)_2$ ($0 \le x \le 3$), where progressive substitution of barium by strontium provokes a decrease of the unit cell parameters a, c and V (Table 1), the results led to the following equations with very high correlation coefficients:

$$a = 5.7868 - 0.0543x \quad R^2 = 0.9967$$
$$c = 21.297 - 0.4029x \quad R^2 = 0.9995$$
$$c/a = 3.6807 - 0.0361x \quad R^2 = 0.9976$$
$$V = 617.28 - 22.445x \quad R^2 = 0.9992$$

where x is the amount of strontium substituting barium and R^2 is the correlation coefficient.

This decrease in all unit cell parameters is in favour of the occupation of 3a and 6c sites by strontium (ri = 1.36 Å in coordination 10 and 1.44 Å in coordination 12) which has a shorter ionic radius than the barium (ri = 1.52 Å in coordination 10 and 1.61 Å in coordination 12) [20]. The results showed the existence of a continuous solid solution in the domain $0 \le x \le 3$. The linear decrease of the lattice parameters when barium is replaced by strontium shows that Vegard law is verified and indicates clearly that there is a complete solubility and so that these compounds form a solid solution in which a given proportion of Ba^{2+} replaces an equal proportion of Sr^{2+}.

Indexing of the X-ray powder diffraction pattern of seven compositions of $Ba_{3-x}Sr_x(VO_4)_2$ ($x=0$, 0.5, 1, 1.5, 2, 2.5 and 3) was performed. The complete powder diffraction data set and intensities are given in Table 2. Intensities given in these tables are obtained from the observed intensities of the Rietveld refinements.

3.2. Resolution of the structure

The structural refinements of $Ba_{3-x}Sr_x(VO_4)_2$ ($0 \le x \le 3$) have been done on powder data by the Rietveld method. The X-ray powder patterns were fitted to the calculated ones using a full-profile analysis program [16] to minimize the profile discrepancy factor $Rp = \Sigma(yi - yci)/\Sigma yi$, where yi and yci are the observed and calculated values at the ith position, respectively. The refinements of $Ba_{3-x}Sr_x(VO_4)_2$ were done starting with the data in ref. [13]. The calculations were performed in the $R\bar{3}m$ trigonal space group in which Ba_1/Sr_1 were located on the sites 3a, Ba_2/Sr_2 and vanadium cations on the sites 6c, O_1 anions were located on the 6c sites and O_2 on the 18h sites. The substitution takes place at barium sites of both coordinations at the same time. For all the compositions $Ba_{3-x}Sr_x(VO_4)_2$ ($0 \le x \le 3$), the occupancy parameters were refined with the following conditions: $occ(Ba_1) + occ(Sr_1) = 1$, $occ(Ba_2) + occ(Sr_2) = 2$ and $occ(Sr_1) + occ(Sr_2) = x$, $occ(Ba_1) + occ(Ba_2) = 3 - x$. Table 3 lists the refinement conditions, cell parameters and reliability factors. Fig. 3 shows calculated and observed diffraction profiles and the difference between them for all the compounds. Similar results were obtained throughout solid solution series. The resulting data for atomic coordinates and isotropic temperature factors with their estimated standard deviation (e.s.d) are listed in Table 4. Table 5 lists some interatomic distances and angles.

The structure of $Ba_{3-x}Sr_x(VO_4)_2$ consists of a three-dimensional anionic framework constructed of $(Ba_1/Sr_1)O_{12}$, $(Ba_2/Sr_2)O_{10}$ polyhedra linked by triangular faces and VO_4 tetrahedra where the VO_4 tetrahedra are isolated from each other (Fig. 4). $(Ba_1/Sr_1)O_{12}$ polyhedra are linked to each other by edges and form layers parallel to *xoy* (Fig. 5). The $(Ba_1/Sr_1)O_{12}$ polyhedron shares six triangular faces with six $(Ba_2/Sr_2)O_{10}$, six edges with six surrounding $(Ba_1/Sr_1)O_{12}$ and six edges with six VO_4 tetrahedra. $(Ba_2/Sr_2)O_{10}$ polyhedra share square faces and corners and form layers parallel

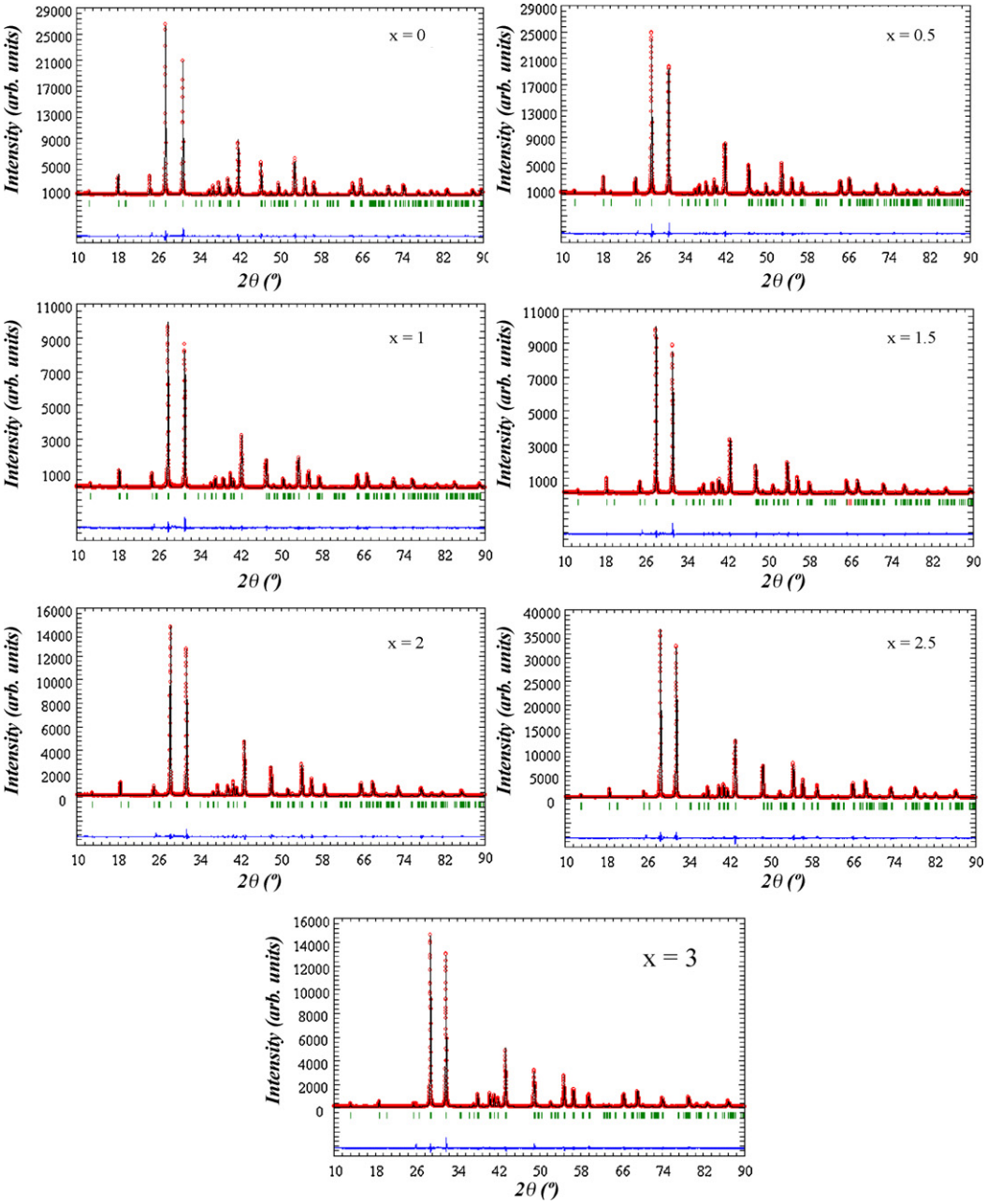

Fig. 3. Final Rietveld plots for $Ba_{3-x}Sr_x(VO_4)_2$ ($0 \le x \le 3$). The upper symbols illustrate the observed data (circles) and the calculated pattern (solid line). The vertical markers show calculated positions of Bragg reflexions. The lower curve is the difference diagram.

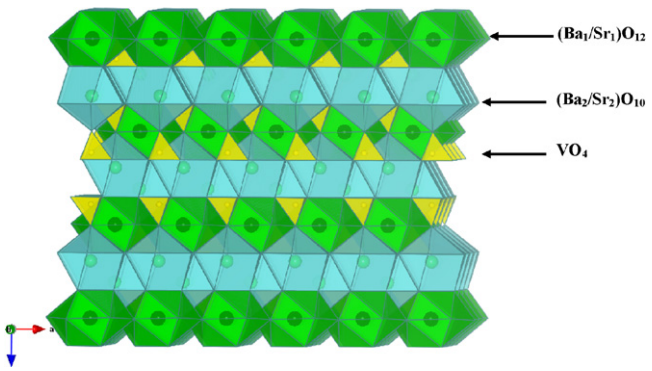

Fig. 4. The structure of $Ba_{3-x}Sr_x(VO_4)_2$ consists of a three-dimensional anionic framework constructed of $(Ba_1/Sr_1)O_{12}$, $(Ba_2/Sr_2)O_{10}$ polyhedra and VO_4 tetrahedra.

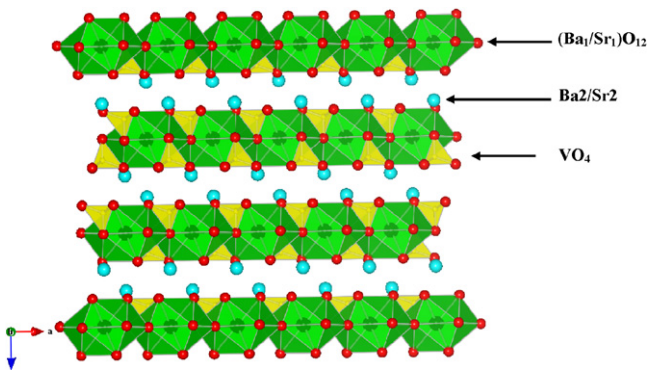

Fig. 5. $(Ba_1/Sr_1)O_{12}$ polyhedra are linked to each other by edges and form sheets along *y* axis.

Table 4
Refined structural parameters for $Ba_{3-x}Sr_x(VO_4)_2$, $0 \le x \le 3$.

	Wyckoff Site	Site symmetry	*X*	*Y*	*Z*	*B*	Occ
$x=0$							
Ba_1	3a	−3m	0	0	0	1.33(4)	1
Ba_2	6c	3m	0	0	0.7948(1)	1.33(4)	2
V_1	6c	3m	0	0	0.5927(2)	0.40(7)	2
O_1	6c	3m	0	0	0.6682(4)	1.71(13)	2
O_2	18h	m	0.4898(5)	0.5102(5)	0.2332(3)	1.71(13)	6
$x=0.5$							
Ba_1	3a	−3m	0	0	0	1.34(3)	0.834(4)
Sr_1	3a	−3m	0	0	0	1.34(3)	0.166(4)
Sr_2	6c	3m	0	0	0.7951(1)	1.34(3)	0.334(4)
Ba_2	6c	3m	0	0	0.7951(1)	1.34(3)	1.666(4)
V_1	6c	3m	0	0	0.5929(1)	0.40(5)	2
O_1	6c	3m	0	0	0.6693(3)	1.65(9)	2
O_2	18h	m	0.4904(3)	0.5096(3)	0.2335(2)	1.65(9)	6
$x=1$							
Ba_1	3a	−3m	0	0	0	1.30(5)	0.691(6)
Sr_1	3a	−3m	0	0	0	1.30(5)	0.309(6)
Sr_2	6c	3m	0	0	0.7956(1)	1.30(5)	0.691(6)
Ba_2	6c	3m	0	0	0.7956(1)	1.30(5)	1.309(6)
V_1	6c	3m	0	0	0.5935(1)	0.45(7)	2
O_1	6c	3m	0	0	0.6694(4)	1.76(12)	2
O_2	18h	m	0.4901 (4)	0.5099 (4)	0.2326(2)	1.76(12)	6
$x=1.5$							
Ba_1	3a	−3m	0	0	0	1.35(4)	0.563(6)
Sr_1	3a	−3m	0	0	0	1.35(4)	0.437(6)
Sr_2	6c	3m	0	0	0.7959(1)	1.35(4)	1.063(6)
Ba_2	6c	3m	0	0	0.7959(1)	1.35(4)	0.937(6)
V_1	6c	3m	0	0	0.5934(1)	0.49(7)	2
O_1	6c	3m	0	0	0.6694(4)	2.13(11)	2
O_2	18h	m	0.4917(4)	0.5083(4)	0.2325(2)	2.13(11)	6
$x=2$							
Ba_1	3a	−3m	0	0	0	1.64(4)	0.383(5)
Sr_1	3a	−3m	0	0	0	1.64(4)	0.617(5)
Sr_2	6c	3m	0	0	0.7963(1)	1.64(4)	1.383(5)
Ba_2	6c	3m	0	0	0.7963(1)	1.64(4)	0.617(5)
V_1	6c	3m	0	0	0.5940(1)	0.73(6)	2
O_1	6c	3m	0	0	0.6701(3)	2.41(10)	2
O_2	18h	m	0.4930(3)	0.5070(3)	0.2325(2)	2.41(10)	6
$x=2.5$							
Ba_1	3a	−3m	0	0	0	1.27(4)	0.188(5)
Sr_1	3a	−3m	0	0	0	1.27(4)	0.812(5)
Sr_2	6c	3m	0	0	0.7970(1)	1.27(4)	1.688(5)
Ba_2	6c	3m	0	0	0.7970(1)	1.27(4)	0.312(5)
V_1	6c	3m	0	0	0.5939(1)	0.38(6)	2
O_1	6c	3m	0	0	0.6724(3)	1.87(8)	2
O_2	18h	m	0.4935(3)	0.5065(3)	0.2329(2)	1.87(8)	6
$x=3$							
Sr_1	3a	−3m	0	0	0	1.36(5)	1
Sr_2	6c	3m	0	0	0.7975(1)	1.36(5)	2
V_1	6c	3m	0	0	0.5945(1)	0.04(6)	2
O_1	6c	3m	0	0	0.6749(3)	2.06(8)	2
O_2	18h	m	0.4941(3)	0.5059(3)	0.2333(2)	2.06(8)	6

to *xoy* (Fig. 6), in other words parallel to $(Ba_2/Sr_2)O_{12}$ polyhedra layers. Fig. 7 shows that each $(Ba_2/Sr_2)O_{10}$ polyhedron is surrounded by six others sharing corners and also shares the three square faces with three corners linked $(Ba_2/Sr_2)O_{10}$. The $(Ba_2/Sr_2)O_{10}$ polyhedron is also surrounded by four $(Ba_1/Sr_1)O_{12}$ polyhedra sharing triangular faces. The $(Ba_2/Sr_2)O_{10}$ is surrounded by three VO_4 tetrahedra by edges and four VO_4 tetrahedra by corners (Fig. 8) and the $(Ba_1/Sr_1)O_{12}$ polyhedron shares six edges with six VO_4 tetrahedra

Table 5
Interatomic distances and angles for $Ba_{3-x}Sr_x(VO_4)_2$, $0 \le x \le 3$.

	$x=0$	$x=0.5$	$x=1$	$x=1.5$	$x=2$	$x=2.5$	$x=3$
$6Ba_1/Sr_1–O_1$	3.338(1)	3.327(1)	3.312(1)	3.296(1)	3.280(1)	3.264(1)	3.229(1)
$6Ba_1/Sr_1–O_2$	2.776(4)	2.745(3)	2.741(3)	2.710(3)	2.680(3)	2.650(3)	2.633(3)
$1Ba_2/Sr_2–O_1$	2.670(9)	2.655(6)	2.637(8)	2.617(8)	2.585(6)	2.527(6)	2.481(6)
$3Ba_2/Sr_2–O_2$	2.858(4)	2.830(3)	2.789(4)	2.749(4)	2.713(3)	2.682(3)	2.656(3)
$6Ba_2/Sr_2–O_2$	2.954(2)	2.945(2)	2.929(3)	2.915(3)	2.901(2)	2.890(2)	2.879(2)
$1V–O_1$	1.621(9)	1.613(7)	1.587(9)	1.573(9)	1.558(7)	1.591(7)	1.607(6)
$3V–O_2$	1.667(3)	1.661(2)	1.661(3)	1.666(3)	1.673(2)	1.665(2)	1.653(2)
$3O_1–V–O_2$	109.6(6)	109.3(4)	110.3(6)	110.0(6)	110.1(4)	109.7(4)	110.0(4)
$3O_2–V–O_2$	109.4(3)	109.6(2)	108.6(2)	108.9(2)	108.8(2)	109.2(2)	109.0(2)

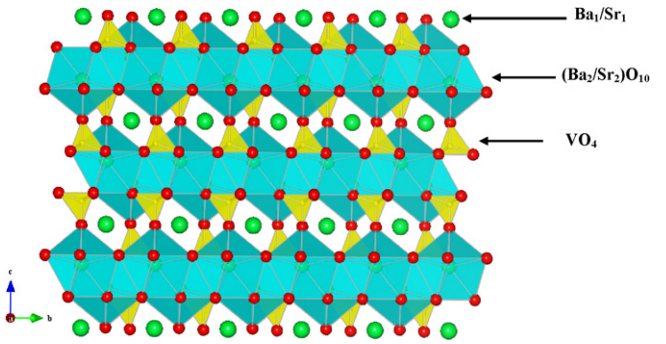

Fig. 6. $(Ba_2/Sr_2)O_{10}$ polyhedra form sheets along *y* axis. $(Ba_2/Sr_2)O_{10}$ polyhedra share square faces and corners and form layers parallel to *xoy*.

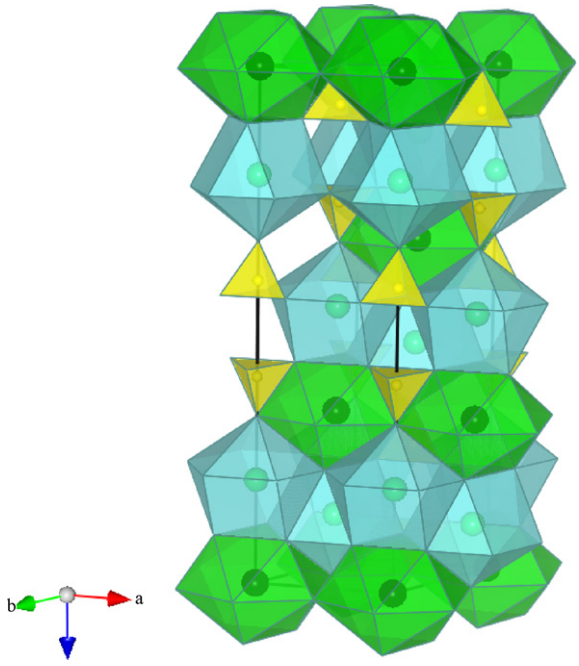

Fig. 7. Three $(Ba_2/Sr_2)O_{10}$ polyhedra share corners and on the top of them one $(Ba_2/Sr_2)O_{10}$ polyhedron shares three square faces.

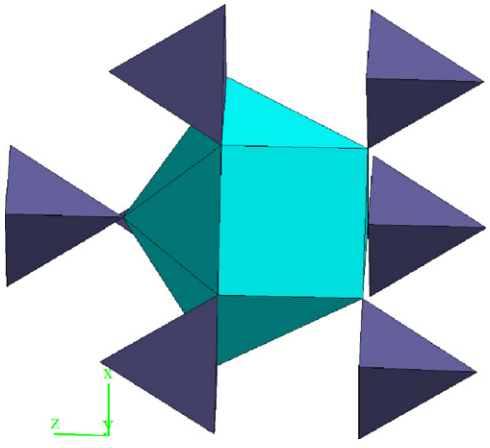

Fig. 8. $(Ba_2/Sr_2)O_{10}$ polyhedron is linked to three VO_4 by edges and to four VO_4 by corners.

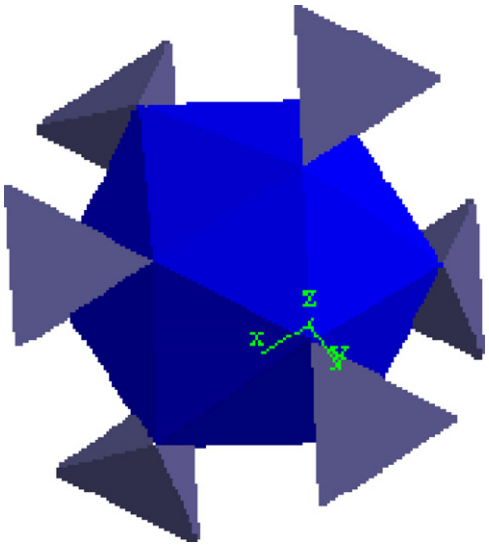

Fig. 9. $(Ba_1/Sr_1)O_{12}$ polyhedron shares six edges with six VO_4 tetrahedra.

(Fig. 9). Each VO_4 tetrahedron is surrounded by three $(Ba_2/Sr_2)O_{10}$ and three $(Ba_2/Sr_2)O_{12}$ sharing edges and by three $(Ba_2/Sr_2)O_{10}$ sharing corners.

3.3. Raman spectroscopy

A factor group analysis of the VO_4^{3-} predicts, for internal modes of $Ba_3(VO_4)_2$ and $Sr_3(VO_4)_2$, the following: three Raman-active stretching modes: A_{1g}, $A_{1g} + E_g(\nu_3)$ and three IR-active modes: $A_{2u}(\nu_1)$, $A_{2u} + E_u(\nu_3)$; and three Raman-active bending modes: $E_g(\nu_2)$, $A_{1g} + E_g(\nu_4)$ and three IR-active modes: $E_u(\nu_2)$, $A_{2u} + E_u(\nu_4)$. The external modes consist of the translational modes of the Ba^{2+}, Sr^{2+}, and VO_4^{3-} ions as well as librations of VO_4^{3-} ions. Vibrational analysis of the external modes leads to: VO_4^{3-} translations: $A_{1g}(R) + E_g(R) + A_{2u}(IR) + E_u(IR)$; $Ba^{2+}{}_1/Sr^{2+}{}_1$ translations: $A_{2u}(IR) + E_u$ (IR); $Ba^{2+}{}_2/Sr^{2+}{}_2$ translations: A_{1g} (R) + $E_g(R) + A_{2u}(IR) + E_u(IR)$; and VO_4^{3-} librations: $A_{2g}(O) + E_g(R) + A_{1u}(O) + E_u(IR)$. The sum of the external modes is: 2 A_{1g} (R) + 3 E_g (R) and 3 A_{2u} (IR) + 4 E_u (IR).

According to XRD investigations reported in this work, the structure remains similar for all the compositions, which should result in the same number of Raman and infrared active bands within the series. Fig. 10 shows Raman spectra of the $Ba_{3-x}Sr_x(VO_4)_2$ $(0 \le x \le 3)$ series. In the Raman spectra of the solid solution series, the V–O stretching vibrations (in the region between 700 and 900 cm^{-1})

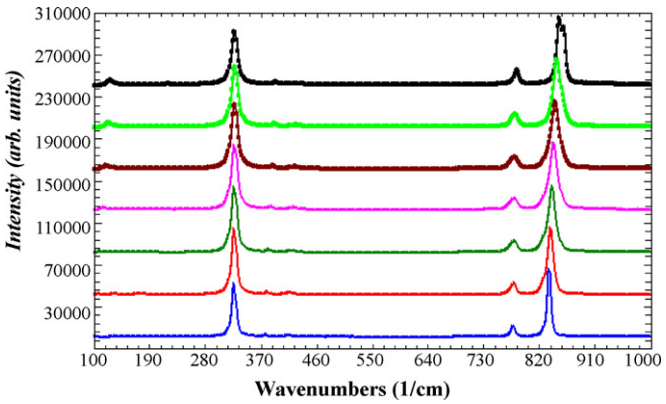

Fig. 10. Raman spectra of $Ba_{(3-x)}Sr_x(VO_4)_2$ $(0 \le x \le 3)$ recoded at 293 K, bottom spectrum ($x = 0$) and upper spectrum ($x = 3$).

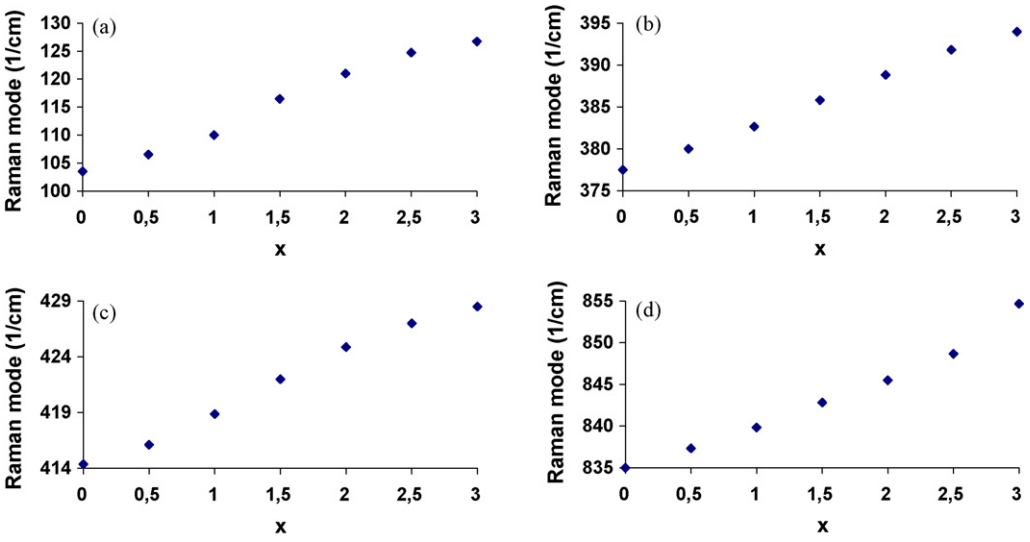

Fig. 11. Composition dependence of some lattice (a) bending (b, c) and stretching (d) modes.

appear with two well resolved bands for all compositions except for $Sr_3(VO_4)_2$ where three bands are observed in agreement with group factor analysis, the third band was not observed in the other compositions and is due to overlapping of the bands. These bands are assigned to symmetrical and asymmetrical stretching vibrations, ν_1 and ν_3. The asymmetrical and symmetrical bands of bending vibrations are predicted to be in the region between 500 and 300 cm^{-1}, the three predicted modes are observed in the Raman spectra. The bands observed below 300 cm^{-1} are attributed to the external modes. Factor group analysis leads to five Raman and seven IR active external modes for $Ba_3(VO_4)_2$ and $Sr_3(VO_4)_2$ and their solid solutions. In the Raman spectra of all the compositions three to four of the five predicted Raman bands were observed.

3.3.1. Stretching vibrations

The 835 and 777.4 cm^{-1} stretching vibrations observed in $Ba_3(VO_4)_2$ show shifts of 20 to 855 cm^{-1}, and 6 to 783 cm^{-1}, respectively, in $Sr_3(VO_4)_2$. These modes exhibit monotonous shifts while the amount of strontium is increased. However, the lowering of wavenumbers when one passes from $Sr_3(VO_4)_2$ to $Ba_3(VO_4)_2$ is relatively weak, which suggests that the frequency is not solely determined by the molar mass of the cation. The assumption of a mode of rotation (or a complex mode of translation-rotation) would probably account for the experimental facts.

3.3.2. Bending vibrations

In the Raman spectra, the two expected bands for the asymmetrical bending vibrations (ν_4) were observed and the frequencies increase from 377.5 and 414.3 cm^{-1} in $Ba_3(VO_4)_2$ to 394 and 428.5 cm^{-1}, respectively, in $Sr_3(VO_4)_2$. The symmetrical band (ν_2) at 325.9 cm^{-1}, in $Ba_3(VO_4)_2$, was observed in all Raman spectra with a slight increase in wavenumbers with increasing strontium content to 327.1 cm^{-1} in $Sr_3(VO_4)_2$.

3.3.3. Lattice modes

Translational modes of a cation against an anion are most readily identified by their strong dependence on the cation mass. These are often strong in IR absorption and weak in Raman scattering and may be observed as broad bands. In the Raman spectra the bands observed at 103.5 and 169 cm^{-1} in $Ba_3(VO_4)_2$ show a large

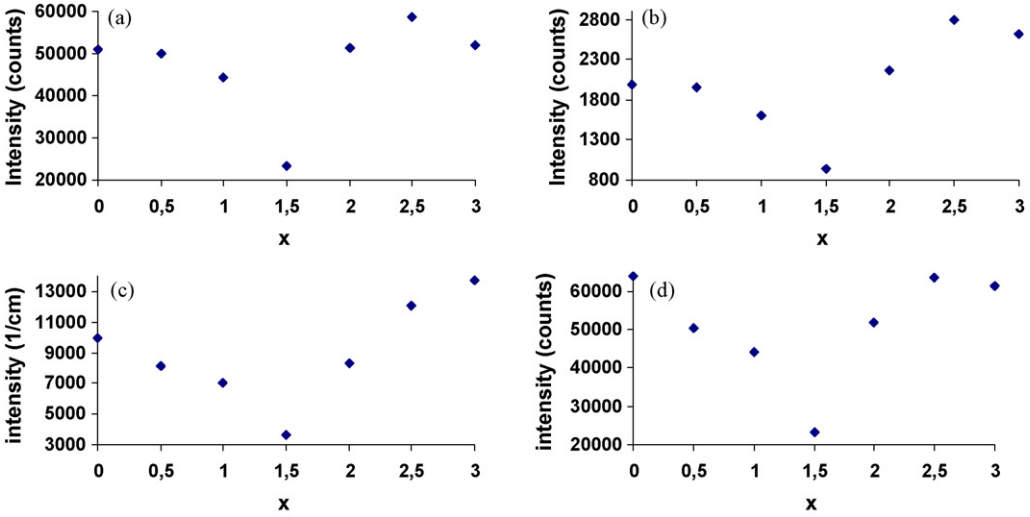

Fig. 12. Intensity variation for 325 cm^{-1} (a), 377 cm^{-1} (b), 777 cm^{-1} (c) and 835 cm^{-1} (d) Raman modes as a function of composition of strontium.

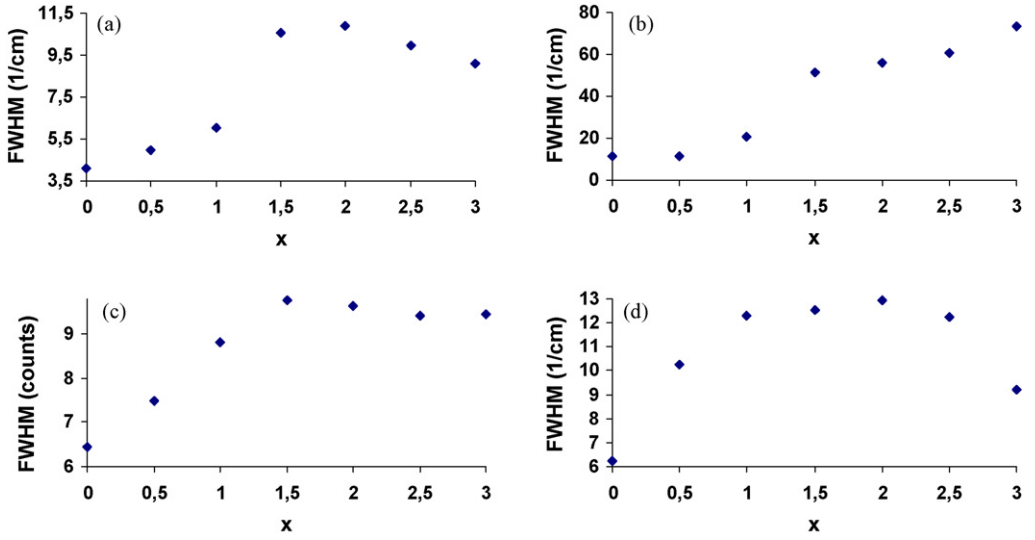

Fig. 13. FWHM behaviour for 103 cm^{-1} (a), 169 cm^{-1} (b), 777 cm^{-1} (c) and 835 cm^{-1} (d) Raman modes as a function of composition of strontium.

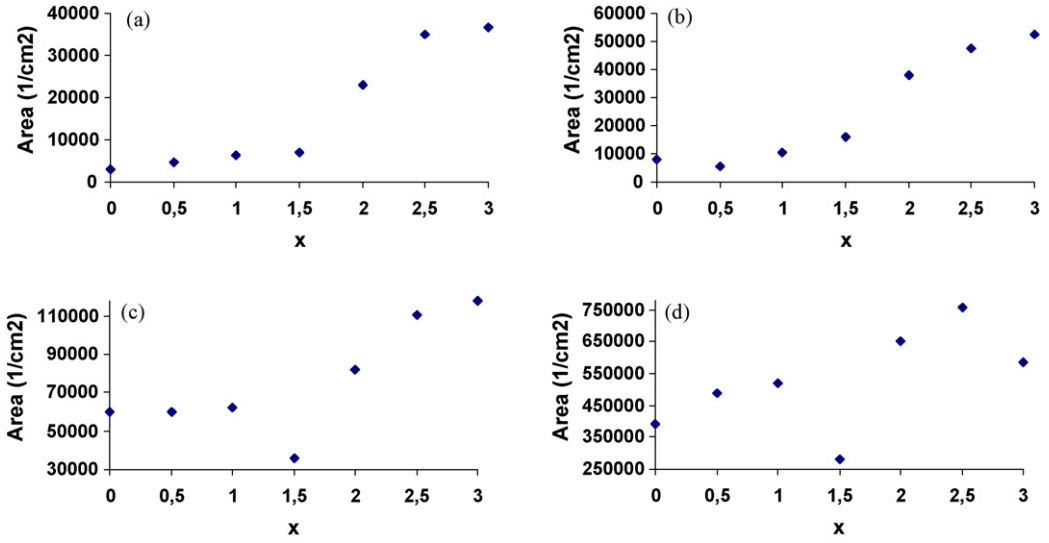

Fig. 14. Area variation for 103 cm^{-1} (a), 169 cm^{-1} (b), 777 cm^{-1} (c) and 835 cm^{-1} (d) Raman modes as a function of composition of strontium.

shift to 126.8 and 199 cm^{-1}, respectively, in $Sr_3(VO_4)_2$, so these bands can be attributed to the translations of Ba_2/Sr_2 cations as the Ba_1/Sr_1 translations are not active modes in the Raman. A Raman band centred at 132 cm^{-1} in $Ba_3(VO_4)_2$ shift only to 134 cm^{-1} in $Sr_3(VO_4)_2$, so this band can be attributed to the translations of VO_4.

The most significant shifts in the observed Raman-active modes with strontium content are plotted for $Ba_{3-x}Sr_x(VO_4)_2$ ($0 \le x \le 3$) in Fig. 11. The progressive substitution of barium by strontium provokes a strong increase in wavenumbers of the bands in all regions. All the modes exhibit monotonous shifts while strontium amount is increased (Fig. 11). This increase can be attributed to the substitution of barium with a molar mass of 137 g/mol by strontium with smaller molar mass of 88 g/mol, same behaviour was observed for these bands in ref. [15]. The broadening of the bands in the vibrational spectra is illustrated in Fig. 12. The curves show that when the strontium amount increase it is accompanied by an increase in full width at half maximum FWHM until $x = 1.5$ and then decreases. This behaviour is due to the statistical distribution of Ba and Sr in the same crystallographic sites [14], this distribution is maximum at $x = 1.5$. At this composition Figs. 13 and 14 show a clear break in the curve of intensities and band areas as a function of amount of strontium, again showing the huge statistical distribution of Ba/Sr in both sites at the medium composition.

4. Conclusions

In this paper we reported the results of the synthesis, crystal chemistry, Rietveld refinements and Raman spectroscopy studies of a new solid solution series, $Ba_{(3-x)}Sr_x(VO_4)_2$ ($0 \le x \le 3$). The existence of a continuous solid solution is confirmed by X-ray diffraction as well as Raman spectroscopy. These materials crystallise in the hexagonal system with $R\bar{3}m$ space group. The structure consists of a three-dimensional framework consisting of $(Ba/Sr)_{(1)}(VO_4)_2^{4-}$ layers linked into a crystal network by $(Ba/Sr)^{2+}_{(2)}$ cations. The vibrational spectra of this crystalline orthovanadate solid solution series are interpreted by means of factor group analysis in terms of space group $R\bar{3}m$. Assignments of the V–O vibrational stretching and bending modes, as well as some of the external modes, have been made. All the modes show a monotonous shift as a function of the composition x. A break in the curves of intensities, full width at half maximum and band areas as a

function of x is observed and attributed to the statistical distribution of Ba and Sr in the same crystallographic sites.

Acknowledgements

The authors are grateful to the Swedish Research Council and the Swedish International Development Co-operation Agency (Sida) for the financial grant (MENA) offered in support of this work.

References

[1] A.A. Fotiev, B.K. Trunov, V.D. Zhuravlev, Nauka Moskva (1985) (in Russian).
[2] L.D. Merkle, A. Pinto, H. Verdun, B. McIntosh, Appl. Phys. Lett. 61 (1992) 2386.
[3] B. Buijsse, J. Schmidt, I.Y. Chan, D.J. Singel, Phys. Rev. B 51 (1995) 6215.
[4] V.D. Zhuravlev, A.A. Fotiev, B.V. Shulgin, Izv. Akad. Nauk SSSR Neorg. Mater. 15 (1979) 2003.
[5] V.D. Zhuravlev, A.A. Fotiev, Zh. Neorg. Khimii. 25 (1980) 2560.
[6] L.V. Kristallov, A.A. Fotiev, Zh. Neorg. Khimii. 26 (1981) 2718.
[7] P. Roux, G. Bonel, Rev. Chim. Miner. 22 (1985) 767.
[8] S. Ni, X. Wang, G. o Zhou, F. Yang, J. Wang, D. He, J. Alloys Compd. 491 (2010) 378–381.
[9] S. Cao, Y. Ma, C. Quan, W. Zhu, K. Yang, W. Yin, G. Zheng, M. Wu, Z. Sun, J. Alloys Compd. 487 (2009) 346–350.
[10] R. Umemura, H. Ogawa, A. Yokoi, H. Ohsato, A. Kan, J. Alloys Compd. 424 (2006) 388–393.
[11] M. Sobczyk, J. Lumin. 129 (2009) 430–433.
[12] W. Carrillo-Cabrera, H.G. von Schnering, Z. Krist. 205 (1993) 271.
[13] P. Süsse, M.J. Buerger, Z. Krist. 134 (1970) 161.
[14] B. Manoun, L. Popovic, D. De Waal, Powder Diffract. 18 (2) (2003) 122.
[15] L. Popovic, B. Manoun, D. De Waal, J. Alloys Compd. 343 (2002) 82.
[16] J. Rodriguez-Carvajal, Collected Abstracts of Powder Diffraction Meeting, Toulouse, France, 1990, p. 127.
[17] T. Roisnel, J. Rodriguez-Carvajal, Mater. Sci. Forum 378 (2001) 118.
[18] M. Azdouz, B. Manoun, M. Azrour, L. Bih, L. El Ammari, S. Benmokhtar, P. Lazor, J. Mol. Struct. 963 (2010) 258.
[19] A. Boultif, D. Louër, J. Appl. Crystallogr. 24 (1991) 987.
[20] R.D. Shannon, Acta Crystallogr. A32 (1976) 751.